Cellulose Nanocomposites From Pentaclethra Macrophylla Benth POD: Synthesis and Adsorption Studies

Nwakaego Orjioke

nwakaego.orjioke@unn.edu.ng

University of Nigeria

Paul-Madus Ejikeme

University of Nigeria

Research Article

Keywords: Acid hydrolysis, Characterization, Cellulose, Cellulose nanocomposites, Pentaclethra macrophylla Benth, Adsorption

Posted Date: July 1st, 2025

DOI: https://doi.org/10.21203/rs.3.rs-6848058/v1

Additional Declarations: No competing interests reported.

CELLULOSE NANOCOMPOSITES FROM PENTACLETHRA MACROPHYLLA BENTH POD: SYNTHESIS AND ADSORPTION STUDIES

Orjioke, Nwakaego Marytheresa *[1], Ejikeme, Paul Madus [2]

[1]Department of Science Laboratory Technology, University of Nigeria, Nsukka
[2]Department of Pure and Industrial Chemistry, University of Nigeria, Nsukka
nwakaego.orjioke@unn.edu.ng; Paul.ejikeme@unn.edu.ng
Correspondence: nwakaego.orjioke@unn.edu.ng

ABSTRACT

Global pollution, progressive industrialization and the increasing world populace have led to severe environmental problems including water pollution. In this study, *Penthaclethra macrophylla benth* (oilbean) pod has been suggested as a possible inexpensive adsorbent for the synthesis of cellulose nanocrystals, for the effective removal of lead at low concentrations, with less post-treatment waste. The synthesized sample was analyzed using X-ray powder diffraction (XRD), Scanning electron microscopy (SEM), Energy dispersive x-ray diffraction (EDX), Transmission electron microscopy (TEM) and Fourier transform infrared (FT-IR) spectroscopy. FTIR spectra revealed many peaks indicating the effective attachment of functional groups containing hydroxyl and oxygen for cellulose nanocrystals. Intense peaks at $2\theta = 12.4^o$, 20.3^o and 26.4^o represent the typical cellulose-I structure. Surface morphology identified by SEM images revealed a stacked flake-like structure while transmission electron micrographs, indicates clusters of spherical shaped nanoparticles, with particle sizes between 1nm – 10 nm. The peaks in the EDX spectra for carbon, oxygen, and other trace elements corresponded to their respective binding energies. To ascertain the kinetics and rate-determining step of the adsorption processes, experimental data were fitted into the pseudo-first order, pseudo-second order, intraparticle diffusion, and elovich models. Adsorption isotherm modelling showed a favourable heterogeneous adsorption as Freundlich isotherm gave a better linear fit. Thermodynamics study showed that the reaction process is feasible and spontaneous.

Keywords: Acid hydrolysis, Characterization, Cellulose, Cellulose nanocomposites, *Pentaclethra macrophylla Benth*, Adsorption.

1.0 INTRODUCTION

The persistent infiltration of dyes, chemical substances, harmful heavy metals, and pharmaceuticals into the environment has become a global environmental issue [1,2]. Heavy metals released into water through household products, pesticides, fertilizer application, sewage disposal, industrial wastewaters, weathering, and release of hazardous underground waste into lakes, rivers, streams, and water bodies, are responsible for the most widespread risks associated with clean water [3-5]. It is therefore becoming challenging to clean up wastes generated during industrial, domestic, and agricultural activities, especially in developing countries, where low economic power makes it difficult to establish safe water treatment processes [6,7].

Among the numerous contaminants found in water, Pb (II) ion requires special attention because of its toxicity, non-biodegradability, accumulation and presence in wastewater from a variety of sectors, including ceramics, mining, metal plating, painting, smelting, weaponry, and refinery operations [8,9]. Lead poisoning in humans may cause anemia, reduction in hemoglobin formation, severe damage to the kidney, nervous system, reproductive system, liver, and brain [10- 12]. The maximum tolerable limit for Pb (II) in drinking water according to the current US Environmental Protection Agency (EPA) standard is 0.015 mg L^{1} [13]. Therefore, its removal have received massive attention due to the potential threat it poses to human health, aquatics, and the ecosystem [14].

Cellulose, a sustainable biodegradable material with low density, good mechanical properties and low toxicity, has been of great research interest recently, due to its potentials as nano-reinforcing filler in polymer nanocomposites, in protective coatings, filtration systems, tissue, antimicrobial films, pharmaceuticals, etc. [15,16]. Cellulose is a widely found polymer made up of β-1,4-linked anhydro-D-glucose units, which contains hydroxyl (-OH) groups [17-18]. Cellulose nanocrystals (CNCs), a highly crystalline nanoscale material produced from cellulose and dispersed in nanomaterials to form nanocomposites have superior properties and improved performance, such as permeability and selectivity [19,20]. However, plant-based cellulose has been utilized recently for the synthesis of nanocrystalline material [21].

The annual quantity of agricultural trash produced by developing countries with Nigeria topping the list has demonstrated their struggles to imitate the global trend of recycling [22,23]. African oil bean (*Pentaclethra macrophylla* Benth) seed pods is an agro waste, carelessly littered in the eastern region of Nigeria, thereby contributing to environmental pollution. *Pentaclethra macrophylla* seed pods were employed herein for the synthesis cellulose nanocrystals, for the removal of lead ion in water.

However, the removal of toxic materials from aqueous solutions using conventional methods (precipitation, filtration, ion exchange, electrochemical treatment, membrane technologies, and evaporation, among others) are ineffective and capital intensive, due to the formation of sludge and secondary pollutants [24-26]. Of these methods, adsorption is one of the most extensively used techniques because of its low cost and simple process [27-28]. Therefore, it is a necessity to develop novel, cellulose nanocomposite materials that can adsorb toxic metals for sustainable and environmentally friendly development.

In this study, the feasibility of using oil bean pod for the synthesis of cellulose nanocrystals, for the removal of lead (II), dissolved in water is investigated. The new obtained system dispersed in polymer matrixes could be a beneficial solution for toxic metal adsorption and other useful industrial purposes.

2. EXPERIMENTAL

2.1 Materials

Penthclethra macrophylla (Oil bean) pods were sourced locally from ‘Ibagwa- Aka’, in ‘Nsukka’ local government area of Enugu State, Nigeria, and used for the synthesis of cellulose nanocrystals. All reagents used were pure and of analytical grade. Sulphuric acid, hydrochloric acid, phosphoric acid, hydrogen bromide, sodium chlorite, acetic acid, nitric acid, potassium hydroxide, sodium hydroxide, Polylactic acid and Multi walled carbon nanotubes were all acquired and used without further purification.

2.2 SYNTHESIS OF CELLULOSE

2.2.1 Isolation of Cellulose

Oilbean pods were washed and sun dried to remove impurities and waxy substances from their external surfaces according to the method described by Liu et al. [29]. 100 g of the dried, grounded and sieved pod was dispersed in distilled water (500 mL), stirred for 2 h at 50 ºC and filtered in order to remove soluble extractives in water.

2.2.2 Alkali Pre-treatment

Alkaline treatment was peformed according to the method described by Tibolla et al. [30]. 25 g of the powder each was treated with NaOH (750 ml, 5% w/v) solution for 2 hours at 95 ^{O}C with continuous stirring at the powder/solution ratio of 1: 30. The process was repeated and the obtained filterate was subjected to washing to remove excess NaOH, before drying.

2.2.3 Bleaching

Partial delignification was performed in order to facilitate extraction and to improve the properties of the acid-extracted cellulose. The resulting solid from previous alkaline treatment was mixed with solution consisting of equal parts (v:v) of acetic acid buffer (27 g NaOH and 75 mL glacial acetic acid, diluted to 1 L with distilled water) and 2 wt% aqueous sodium chlorite, at 80 °C for 3h under continuous stirring. Bleached solids were filtered and washed repeatedly until neutral pH is reached, before drying to constant weight at 105 ºC for 8 h. The resultant dried product was grounded and labelled appropriately for further analysis.

2.3 Synthesis and Purification of Cellulose Nanocrystals (CNCS)

The preparation of cellulose nanocrystals followed the procedures described by Schiavi, et al., [31], with modification. 30 g of the oil bean pods cellulosic source materials was hydrolyzed using 100 mL of 68 wt% H_2SO_4, at 30 °C, and reaction time of 150 min under continuous mechanical stirring with a Teflon coated magnetic bar. The reaction was terminated by adding 100 mL cold distilled water after a pre-determined time, and the suspended substances washed with distilled water using repeated centrifugation cycles of 10 min at 12000 rpm, i.e. the supernatant liquor was removed from the sediment, replaced and washed using distilled water. The centrifugation was stopped when a cloudy suspension is obtained. Dialysis of the suspension against distilled water was conducted at room temperature until a constant pH is obtained and the sample sonicated for 20 min in an ice bath to homogenize the CNC and to avoid overheating, which might cause desulphation. CNC Yield was calculated using the equation below.

$$Yield = \frac{mass\ of\ dried\ CNC}{mass\ of\ pulp} \times 100\% \qquad (1)$$

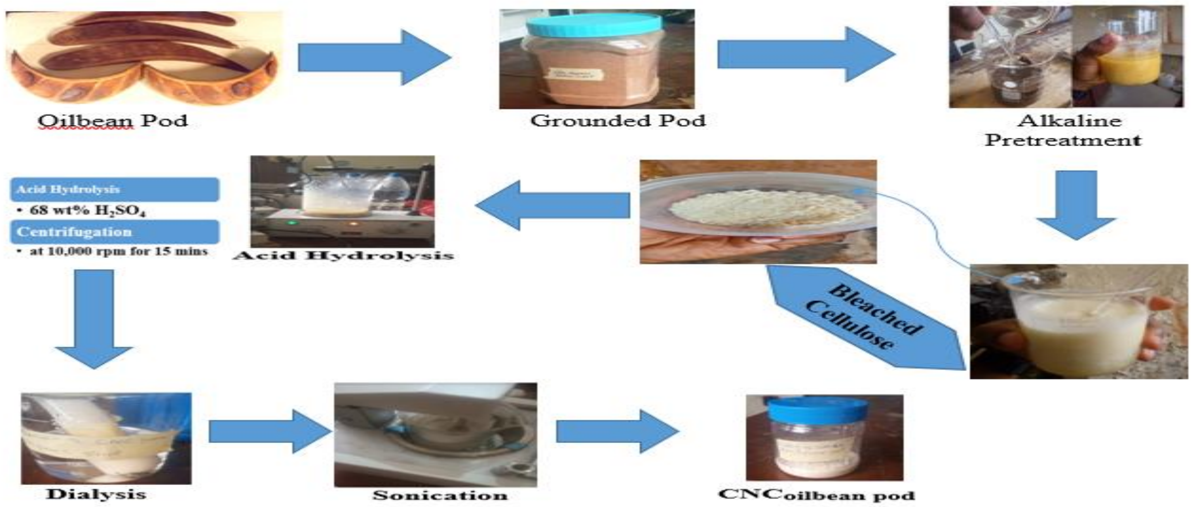

Figure 1: Schematic representation of the synthesis of cellulose and cellulose nanocrystals

2.4 SYNTHESIS of CNCs/GO NANOCOMPOSITE

The experimental procedure for the synthesis of cellulose nanocrystals – graphene oxide was adopted from Junhong, et al.,[32], 20 g of purified CNCs were dispersed and sonicated for 60 min in 200 cm^3 of ethanol. Then 20 g of the synthesized graphene oxide was added to this solution and the resulting mixture sonicated for 80 min. The resultant solution was centrifuged at 5000 rpm for 30 min and the precipitates oven-dried at 100 ºC to obtain CNCs/GO nanocomposite.

2.5 SYNTHESIS of CNCs-GO-PLA-MWCNTs NANOCOMPOSITES

In a 250 cm^3 beaker labeled A, containing 50 cm^3 of acetone/dimethyl acetamide (DMAC) in the ratio of 2:1 v/v %, 200 mg of MWCNTs/ 2 g of PLA were dissolved according to the method proposed by Li, *et al*.,[33] and placed in a sonicator for 30 min at room temperature. 20 g of previously prepared CNCs/GO dispersed in 100 cm^3 of acetone/water in the ratio of 9:1 in a separate 250 cm^3 beaker was labelled B. The solution in beaker B was transferred into beaker A, and stirred to attain a homogenous mixture with further ultra-sonication for 2 h. The resulting dense colloid was dried at 120 ºC for 6 h and all samples stored in the desiccator using sterile air tight containers and labeled appropriately.

2.6 BATCH ADSORPTION STUDIES

2.6.1. Preparation of Adsorbate

Stock solution of lead was prepared by weighing 1.59 g of $PbNO_3$ powder into 250 cm^3 beaker containing 100 mL of deionized water. The solution made up to mark in a 1000 dm^3 volumetric flask with deionised water. Working solutions of the desired concentrations of Pb^{2+} were daily prepared from the stock solutions. Adsorption parameters such as pH, adsorbent dose, contact time, initial concentration and temperature were studied using batch adsorption methods. To study the influence of pH, 20 cm^3 of 100 mg dm^{-3} adsorbate solution was measured 100 mL beakers and 50 mg of adsorbent added to each. The solutions were altered to the required pH using appropriate amounts of 0.1 mol dm^{-3} NaOH or HCl,. agitated for 30 min and left to attain equilibrium for 24 h. The solutions were filtered, and the amount of metal ion adsorbed determined from the difference between the initial and final concentrations. Percentage removal efficiency and sorption capacity (q_e) of Pb^{2+} were calculated using to the equations below.

$$(\frac{Ci-Ce}{Ci})X\ 100 \quad (2)$$

$$(\frac{Ci-Ce}{m})X\ v \quad (3)$$

Where m is the mass of the adsorbent (mg), V is the volume (dm^3) of the adsorbate solution, C_i is the initial concentration of the adsorbate (mg dm^{-3}), C_e is the equilibrium concentration of the adsorbate (mg dm^{-3}), and q_e is the adsorption capacity (mg g^{-1}).

2.6.1.1 Effect of Optimum Parameters

Effect of pH on the sorption of lead ion onto synthesized nanocomposites (GO-CNCs, and GO-MWCNTs-PLA-CNCs) from aqueous solutions were investigated over a pH range of 4-11. For contact time, adsorption experiments were carried out between 30-90 min when other parameters are constant. The influence of increasing adsorbent dosage were investigated over a range of 0.1-0.5g, initial ion concentration were studied over a concentration range of 50 – 400 ppm and the effect of temperature studied over the range of 25 – 45 ^{o}C, when other parameters are constant respectively.

2.6.2 CHARACTERIZATION

The structural changes from oilbean cellulose to CNCs and graphite to graphene oxide were investigated by FTIR spectroscopy using a Nexus Thermo FTIR (ThermoNicolet is10, USA) spectrophotometer. The surface morphology of cellulose and cellulose nanocrystals were investigated using scanning electron microscopy (JOEL- JSM- 7600F, USA) with an accelerating voltage of 15–20 kV. Energy dispersive x-ray (EDX) diffraction was used for the elemental analysis of cellulose nanocrystals. Transmission electron microscopy (TEM) (JOEL- ARM200F-G Verios 460L, USA) was used to determine the dimensions of the CNCs obtained from the oilbean pod. The structural analysis of the samples was studied by X-ray diffraction (XRD) using a (Rigaku D/ MaxIIIC, PW1800) diffractometer with a scanning rate of 5°C per min with Cu Kα radiation source (λ = 1.54060 Å) operating at 40 kV and 15 mA.

2.6.3 ADSORPTION ISOTHERMS and KINETIC STUDIES

Adsorption isotherms are very useful in adsorption capacities analysis. When there is adsorption equilibrium between the amount of adsorbates on the adsorbents and the equilibrium concentrations of adsorbates at constant temperatures, an adsorption isotherm is formed [34]. Various kinds of models, such as the Dubinin–Radushkevich , Temkin's, Langmuir and Freundlich, models etc., are used to determine the adsorption isotherms [35]. Also, adsorption kinetics used to define the mechanism and efficiency of Pb^{2+} on nanocomposites adsorbents were studied by different kinetic models (Pseudo–first order, Pseudo-second order, Elovich, and Intraparticle diffusion models) [36-37].

The Langmuir model is used to indicate monolayer adsorption and the equation is written as follows:

$$Ce/q_e = 1/Q_o b + C_e/Q_o \quad (4)$$

Where Q_o (mg/g) represents the monolayer adsorption capacity of the adsorbent. C_e (ppm) is the equilibrium concentration of lead ion solution, q_e in mg g^{-1}, denotes the equilibrium capacity of lead ion in the adsorbent.

b (L/mg) is the Langmuir bonding energy coefficient while the values of Q_o and b are obtained from the slope and intercept of the plot of Ce /q_e vs C_e.

The Freundlich equation used to describe adsorption on a heterogeneous surface is written as follows:

$$\text{Log } q_e = \log K_f + 1/n \log C_e \quad (5)$$

When K_f represents the adsorption capacity, n is the adsorption intensity. 1/n below 1 indicates a normal adsorption, while above 1 indicates cooperation adsorption. K_f and n values can be obtained from the slope and intercept of plot log q_e vs log C_e .

The Temkin isotherm model represents the uniform distribution of binding energies over surface binding adsorption. Thus, the equation is written as:

$$q_e = B \ln K + B \ln C_e \quad (6)$$

where B = RT/b, b (Temkin constant) is the heat of adsorption, q_e (mg/g) is the amount of metal ion per unit weight of adsorbent, and C_e (ppm) is the metal ion concentration in solution at equilibrium that is unabsorbed. The constants B and K obtained from the plot of q_e vs ln C_e are related to the heat of sorption (J/ mol), and equilibrium binding, respectively.

Dubinin-Radushkevich isotherm is used to express the adsorption mechanism onto a heterogeneous surface with a Gaussian energy distribution, and its linearized equation is written as:

$$\text{Ln } q_e = \ln q_m - BE^2 \quad (7)$$

Where q_m (mg/g) is the adsorption degree, B (mol/kJ) is the adsorption energy, and E is the polanyi potential that obtained by the following equation:

$$E = RT \ln (1+1/C_e) \quad (8)$$

R is the ideal gas constant (R=8.314 J mol^{-1} K^{-1}), T is the absolute temperature (K). B and q_m can be obtained from the plot of ln q_e vs E^2, while mean free energy E (KJ/mol) of adsorption is calculated using the equation below:

$$E = 1/ (2B)\, ½ \quad (9)$$

Where E is used to characterize the adsorption type as physical adsorption when $E < 8$ kJ mol^{-1} , or chemical adsorption whe n E = 8 - 16 kJ mol^{-1}).

Pseudo-first order model is described using to the following equation:

$$\text{Log } (q_e - q_t) = \log q_e - (K_1 /2.303)\, t \quad (10)$$

Where, K_1, is the rate constant, q_e and q_t (mg g^{-1}), are the equilibrium adsorption capacities at the time (t(min)) respectively. K_1 and q_e can obtain from the plot of log (q_e -q_t) vs t plot.

Pseudo-second order model is represented linearly by the equation below:

$$t/q_t = 1/K_2 q_e^2 + 1/q_e\, t \quad (11)$$

where K_2 (g mg^{-1} min^{-1}) is the rate constant. K_2 and q_e is calculated from the linear plot of t/q_t vs t.

Intraparticle diffusion model is used to describe the mechanism of solute transfer involved in adsorption process which can be expressed using the following equation:

$q_t = K_i\ t\ ½ + C$ (12)

K_i (mg g^{-1} $min^{-1/2}$), is the rate constant, C (mg g^{-1}) is the boundary layer effect. Therefore, K_i and C are obtained from a linear plot of q_t vs $t^{1/2}$.

Elovich model is used to describe the activated chemisorption using the equation below:

$q_t = 1/\beta \ln[\alpha\beta] + 1/\beta \ln t$ (13)

where α is the initial adsorption, and β, the coefficient of adsorption.

Adsorption thermodynamics was studied at temperatures 298, 303, 308, 313 and 318 K. and the thermodynamic parameters [Gibbs free energy (ΔG^o), entropy (ΔS^o), and enthalpy (ΔH^o)] were calculated using the following equation:

$K_d = Q_e/C_e$ (14)

$\Delta GO = RTLnK_d$ (15)

$Ln\ K_d = (\Delta S^o /R)-(\Delta H^o /RT)$ (16)

Where R (8.314 J mol^{-1} K^{-1}) is the gas constant and T (K) is the temperature. K_d, is the coefficient of distribution (mL/g), ΔS^o (J/mol K) and ΔH^o (J/mol) were calculated from the slope and intercept of the linear plot of Ln k vs. 1/T. The Gibbs free energy ΔG^o (KJ mol^{-1}) is calculated from the following equation:

$\Delta G^o = \Delta H^o - T\ \Delta S^o$ (17)

3.0. RESULTS AND DISCUSSION

3.1. X-Ray Diffraction Measurements

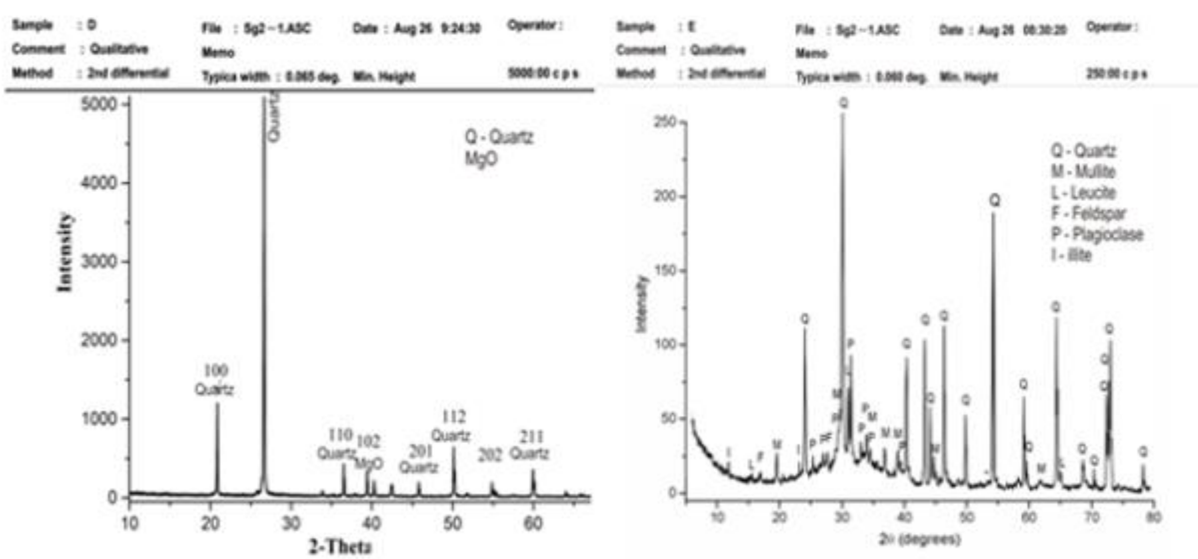

Figure 2: XRD spectra for cellulose (COP) and CNC (CNCOP) oil bean pod

Oilbean pod-CNC showed a unique cellulose I crystalline composition with intense peaks at 2θ = 12.4°, 20.3° and 26.4°. The cellulose crystals exhibit characteristic assignments at 110, and 200 planes, respectively. The crystallinity index of the samples were calculated according to amorphous subtraction method [38]. Increase in crystallinity of cellulose and cellulose nanocrystals from 67% to 79% respectively, could be linked to lignin removal through hydrolysis. These results conform with similar trend as results calculated by [39].

3.2. FOURIER TRANSFORM INFRA-RED STUDIES

The peak assigned at 3204 cm^{-1} - 3414 cm^{-1} represents the stretching and bending vibrations of OH, which corresponds to functional groups attributed to cellulose as seen in figure 4. Typical "finger-prints" of cellulose were also found at 787 cm^{-1} and 785 cm−1, an indication of the presence of β-glycosidic links in the structure of the cellulose and cellulose nanocrystals. Peaks at 1649 and 1641 cm^{-1} is attributed to the stretching vibrations of C-O group, while the bands in the 1035–1160 cm^{-1} range represented the C-O-C stretching of the pyranose ring. After hydrolysis, the insignificant differences between cellulose and cellulose nanocrystals spectra, showed that the chemical characteristics were retained in the CNCs [23]. The absence of peaks at 1735 cm^{-1} in both spectra, is attributed to C=O stretching of the acetyl ester and uronic groups [40]. The overall results indicated that the applied alkali treatment and subsequent acid hydrolysis played a major role in rearranging the crystalline structure of cellulose and in the removal of lignin and hemicelluloses from the raw cellulose matrix.

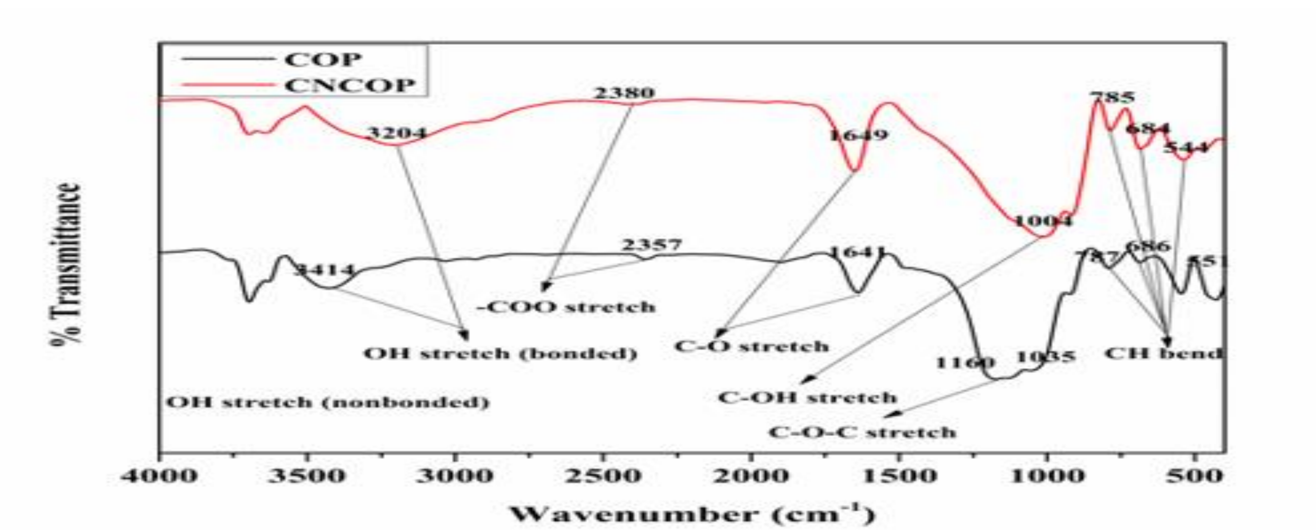

Figure 4: FTIR spectra for cellulose (COP) and CNC (CNCOP) oil bean pod

3.3. SCANNING ELECTRON MICROSCOPY STUDIES

The source of Cellulosic material and hydrolysis method has great influence on the dimension and characteristics of nanocellulose. SEM image of cellulose from oilbean pod (figure 6) shows highly agglomerated rough surface, while that of cellulose nanocrystals shows a stacked flakes -like structure with noticeable size reduction, as a result of the strong hydrogen bonding among the surface hydroxyl groups

[19, 41] . The size reduction after acid hydrolysis is attributed to the successful removal of amorphous phase.

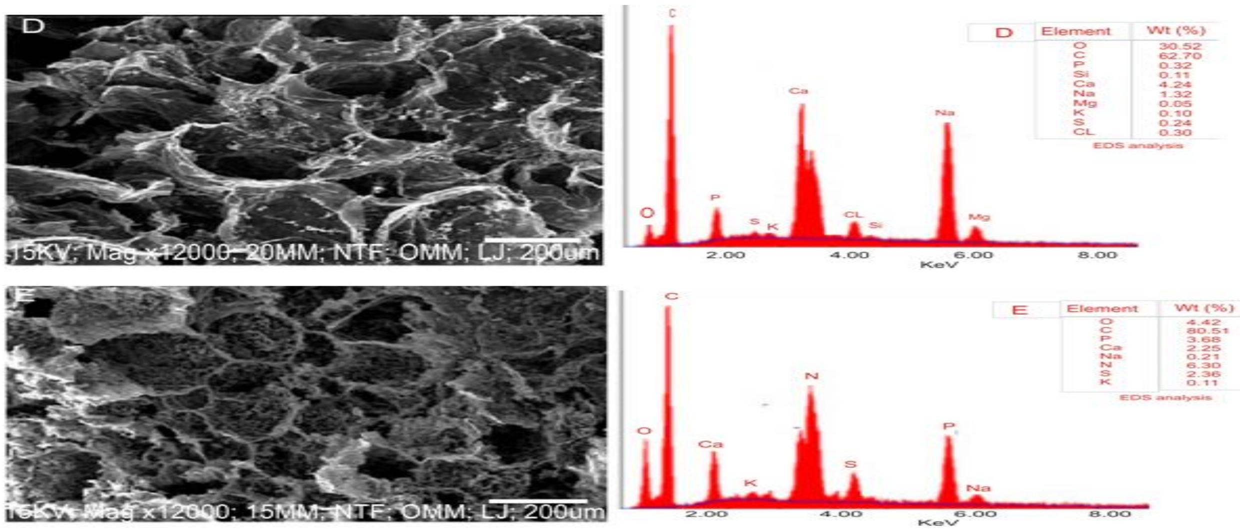

Figure 6: SEM-EDS for Cellulose (D) and CNC (E) oil bean pod

3.4. ENERGY DISPERSIVE X-RAY DIFFRACTION STUDIES

The elemental analysis of CNCs was conducted using energy dispersive x-ray diffraction (EDX) attached with FE-SEM. EDX spectrum (as shown in Figure 6) showed the peaks for carbon, oxygen, and sulphur corresponding to their binding energies, respectively. CNCs contain 2.36-wt% elemental impurity of sulphur along with the main components such as carbon (80.51%) and oxygen (4.42%). This elemental impurity is caused by the acid (H_2SO_4) hydrolysis of cellulose fibers.

3.5. TRANSMISSION ELECTRON MICROGRAPH STUDIES

The morphological studies of cellulose and cellulose nanocrystals shown in Figure 8 using transmission electron micrographs, indicates a cluster of spherically shaped nanoparticles. The presence of pores are significantly visible from the TEM images of cellulose and cellulose nanocrystals. Also,the ultrasonication process might play an important role in the formation of the spherically shaped CNC. This results conformed with the works of Tibolla, et al.[30] and Tao, et al., [38].

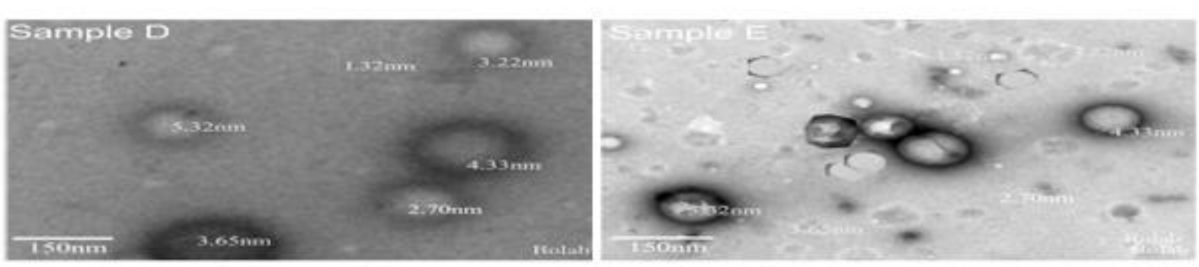

Figure 8: TEM images for Cellulose (D), CNC (E)

3.6. ADSORPTION STUDIES

3.6.1 Effect of pH

The influence of pH on the adsorption of Pb^{2+} was investigated over a pH range of 4-13. Figure 9 shows that the change in pH of the adsorbate solution greatly influenced the extent of removal of Pb^{2+} from aqueous solution. The uptake of Pb^{2+} was low at acidic conditions, but increase in the removal efficiencies was obtained as the solution pH increased. The removal of metal ions is facilitated at basic conditions due to precipitation of metal ions in solution as hydroxo species. This leads to increased removal efficiencies noticed at basic pH conditions. This result is in agreement with the works reported by Lasheen, et al., [42], and Yu, et al., [43].

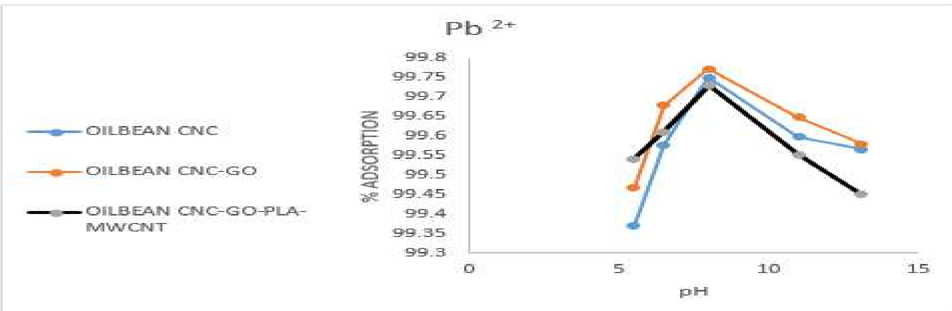

Figure 9: Adsorption of Pb $^{2+}$onto oil bean pod CNC, GO-CNC, and CNC-GO-PLA-MWCNT as a function of pH [conditions: contact time 30 min, agitation speed 150 rpm, temperature 25 ºC, adsorbent dosage 0.1g]

3.6.2 Effect of adsorbent dosage

The influence of varying the adsorbent dose on the adsorption of Pb^{2+} is shown in Figure 10. Adsorbent dosages ranging from 0.1 g - 0.5 g was equilibrated for 24 h, at a fixed concentration. Increase in surface area is influenced by increase in adsorbent dosage, causing additional active sites to become available [44-45]. This explains why increasing the dosage of CNC nanocomposites and cellulose resulted in high removal efficiency for both adsorption processes. Furthermore, in both adsorption processes, the removal efficiency of cellulose and CNC-GO-PLA-MWCNT was greater than that of CNC and CNC-GO, indicating the efficacy of CNC-GO-PLA-MWCNT for the removal of divalent metal ions.

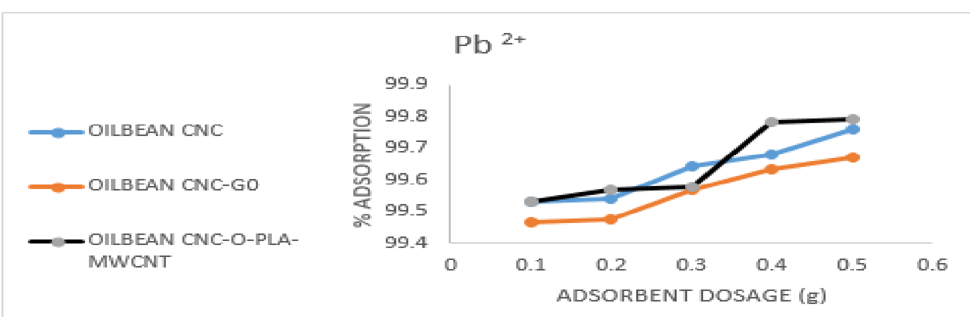

Figure 10: Adsorption of Pb^{2+} onto oil bean pod CNC, GO-CNC, and CNC-GO-PLA-MWCNT, as a function of adsorbent dosage [conditions: contact time 30 min, agitation speed 150 rpm, pH 8.0, equilibrium 24 h]

3.6.3 Effect of contact time

The effect of contact time was investigated over a period of 30- 90 min with the conditions described in Figure 11, using CNC, CNC-GO and CNC-GO-PLA-MWCNT as adsorbents. A steady increase in the removal efficiency was obtained due to the availability of more active sites at the initial stage [27, 46]. As the process continues, adsorption sites become saturated, hence, a state of equilibrium where little or no further increase in removal is reached. Figure 11 showed that equilibrium was achieved at 75 for CNC and CNC-GO-PLA-MWCNT, and at 60 min for CNC-GO adsorbents, for the removal of Pb^{2+}. The removal efficiency could be attributed to the increased surface area, which creates room for more available active sites.

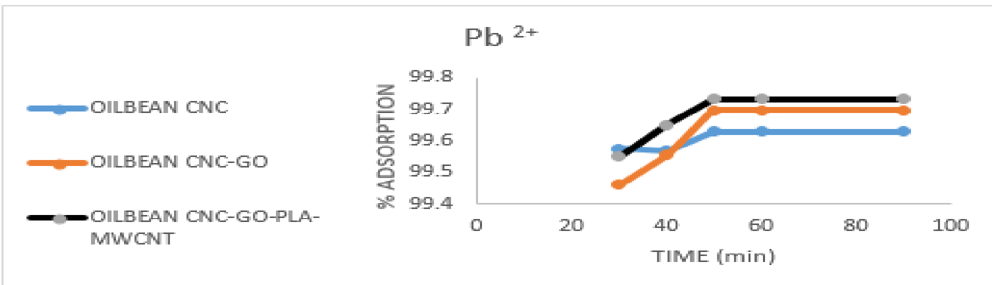

Figure 11: Adsorption of Pb $^{2+}$ onto oil bean pod CNC, GO-CNC, and CNC-GO-PLA-MWCNT as a function of contact time [conditions: adsorbent dosage 0.5 g, agitation speed 150 rpm, temperature 25 ºC, pH 8.0]

3.6.4 Effect of initial concentration

Different concentration ranges with the same amount of adsorbent were utilized in order to explain the increase in each adsorbent's adsorption capacity (q_e). For a given amount of adsorbent, it was found that an increase in adsorbate concentration reduces the percentage of adsorption and raises the adsorption capacity (q_e). Because there are more active sites available on the adsorbent, great removal efficiency can therefore be achieved at lower concentrations. The difference in concentration that forms between the adsorbent's surface and the bulk solution triggers an increase in driving force, which in consequently results in an increase in adsorption capacity as the initial concentration of adsorbate increases [47-48]. Nevertheless, as the process proceeds at higher concentrations, Pb^{2+} molecules saturate the adsorbents' active sites. Therefore, as the concentration is increased, this process results in a decrease in the percentage adsorption and an increase in the adsorbents' intake of the adsorbate (q_e).

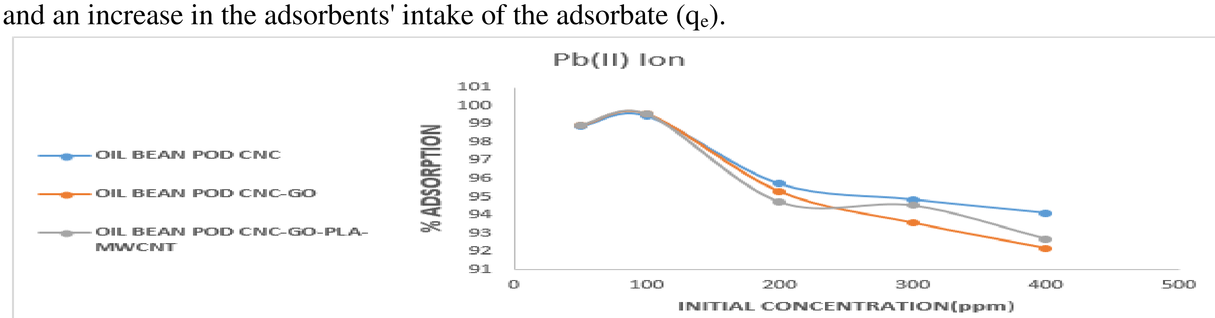

Figure 12: Adsorption of Pb^{2+} onto oil bean pod CNC, GO-CNC, and CNC-GO-PLA-MWCNT as a function of initial concentration [conditions: adsorbent dosage 0.5g, agitation speed 150 rpm, temperature 25 ºC, contact time 90 min, pH 8.0]

3.6.5 Effect of temperature

The influence of the change in temperature was investigated at varying range of 25- 45 ºC. The removal of Pb^{2+} onto CNC, CNC-GO and CNC-GO-PLA-MWCNT, increases with an increase in temperature, which may result in a decrease of solution viscosity and an increase in kinetic energy of the adsorbates onto the adsorbent active sites [43]. These factors also explain why the adsorbates' removal from the pores/sites CNC, CNC-GO, and CNC-GO-PLA-MWCNT is activated, leading to an increase in Pb^{2+} uptake at higher temperatures. The finding explains why these adsorbents might be used to remediate metal-contaminated effluents that are released directly from industrial sources.

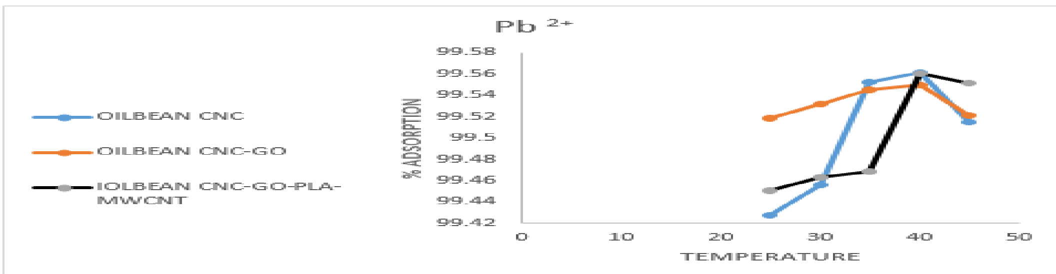

Figure 13: Adsorption of Pb^{2+} oil bean pod CNC, GO-CNC, and CNC-GO-PLA-MWCNT as a function of temperature [conditions: adsorbent dosage 0.5g, agitation speed 150 rpm, pH 8.0, equilibrium 24 h]

ISOTHERM MODELS

Distribution of adsorbate molecules/ions in the solid and liquid phases, mechanisms/interactions involved in adsorption, and the efficacy of adsorbents are all revealed by isotherms [49-52]. The Dubinin-Radushkevich (D-R), Freundlich, Langmuir, and Temkin isotherm models were employed to analyze the experimental data collected for Pb^{2+} adsorption. The results (figure 14) demonstrated that the equilibrium data obtained for Pb^{2+} removal utilizing CNC, CNC-GO, and CNC-GO-PLA-MWCNT were best characterized by the Freundlich model. This suggests that binding strength diminishes with increasing site occupation degree and that the stronger binding sites were occupied first [17].

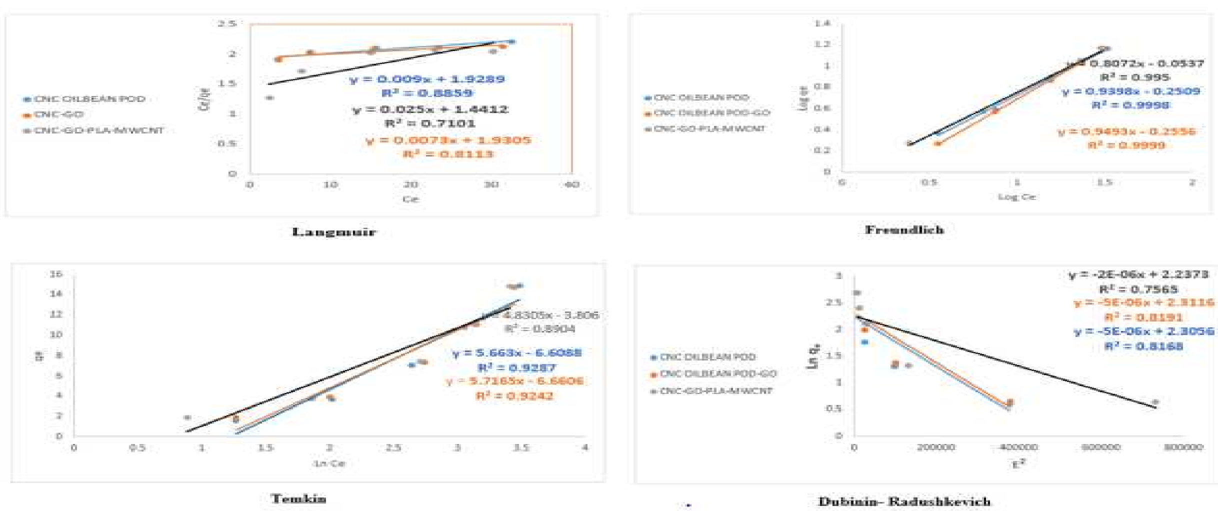

Figure 14: Langmuir, Freundlich, Temkin and Dubinin- Radushkevich isotherm models for the adsorption of Pb ion onto CNC oil bean pod, CNC-GO and CNC-GO-PLA-MWCNT

The dynamics of the system affect the adsorption mechanism's rate-controlling step. The kinetic models used in determining mass transfer and chemical reaction processes, are displayed in Figure 15. Each model's correlation coefficients are plotted, with the best fit being displayed. According to Qiao et al. [53], the pseudo second order kinetic model fits the lead adsorption on CNC/-CNC-GO/ CNC-CNC-GO-PLA-MWCNT the best. As concentration rises, the pseudo second order rate constant (k_2) rises until a peak is achieved [54]. Since the availability of sites has a correlation with the initial concentration of metal ions and the time at which equilibrium adsorption capacity is reached, this could possibly be attributed to a change in the ratio of binding interactions, which also explains the relationship between the number of available binding sites and the rate of adsorption [55]. Since the intercept in the intraparticle diffusion model was not equal to zero, it may be concluded that there are more rate-limiting steps in addition to the complex process that controls the rate.

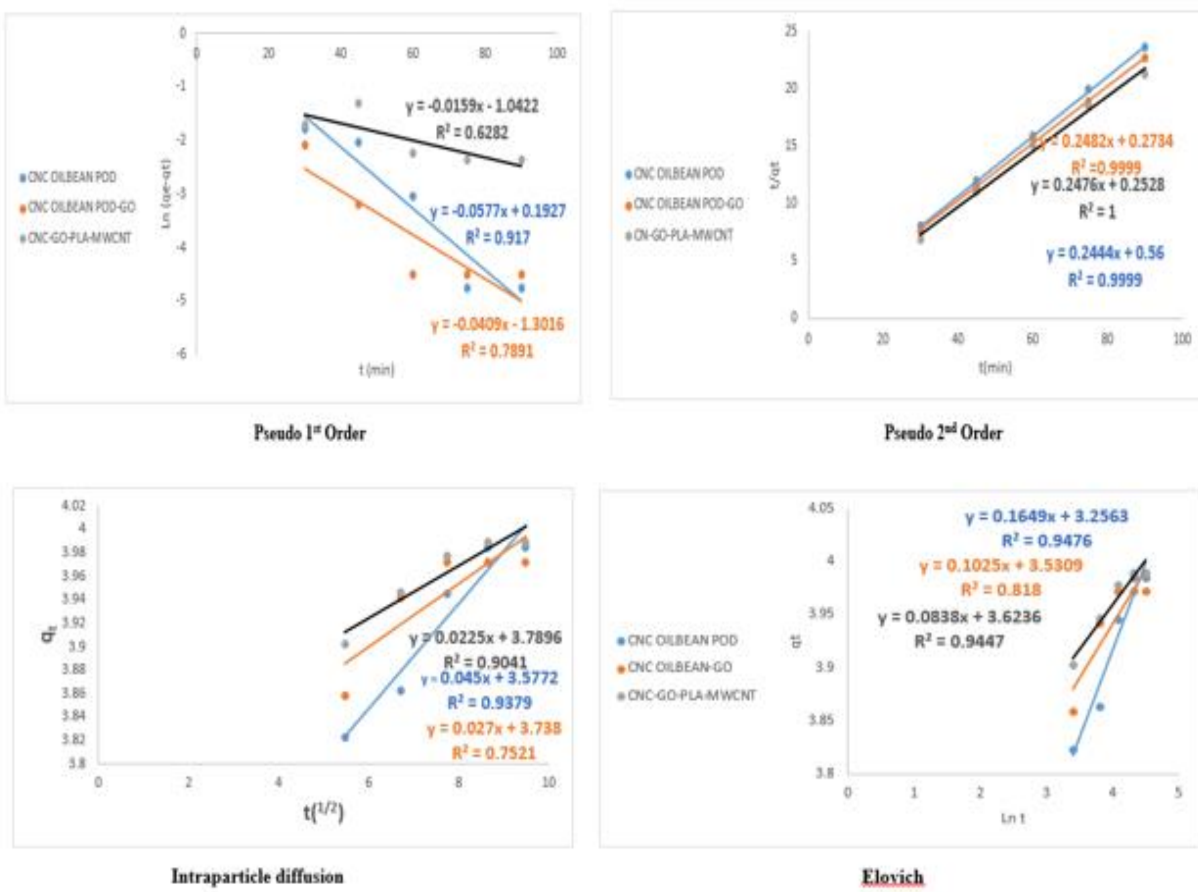

Figure 15: Pseudo 1st Order, Pseudo 2nd Order, Intraparticle diffusion and Elovich plots for Pb ion adsorption onto CNC oilbean pod, CNC-GO and CNC-GO-PLA-MWCNT

The adsorption of Pb (II) ions by CNC, CNC-GO, and CNC-GO-PLA-MWCNT at varying temperatures indicated decreased randomness at the solid-liquid interphase during the sorption processes of lead ion on the adsorbent, as shown by the negative values of entropy change (ΔS°).

This could be as a result increased mobility leading to better breakage of the activation energy barrier, with improved adsorbent penetration, resulting in improved intra-particle diffusion rate (Xu et al., 2020). Adsorption of Pb^{+2} ion onto CNC/ CNC-GO/ CNC-GO-PLA-MWCNT was enthalpy-driven (Farooq et al., 2022). Table 3 displays the predicted thermodynamic parameters for the adsorption of Pb^{2+} ions, which were derived from equations 16 and 17. Pb^{2+} ions undergo a spontaneous adsorption process that generates many products in a forward direction, resulting in negative values of ΔG° for all adsorbents (Sc et al., 2017). An increase in negative values of ΔG° for the adsorption of Pb^{2+} ions by using CNC/ CNC-GO/ CNC-GO-PLA-MWCNT indicates a spontaneous and favourable process at higher adsorbate temperature, which did not require an external energy source for the system (Table 3). This could be the cause of the increased uptake of metal ions from their solutions by the adsorbents with increasing temperature.

The results indicated that the adsorption of Pb^{2+} ion produced positive values for the standard change in enthalpy (ΔH°). This implies that the elimination of Pb^{2+} ions is endothermic. Also, the heat produced by a chemical process (chemisorption) ranges from 80 to 200 kJ mol^{-1}, while the heat evolved during physical adsorption (physisorption) is between 2.1-20.9 kJ mol^{-1}. Therefore, the ΔH° values were more for physisorption and less for chemisorption, confirming that the removal of Pb^{2+} with CNC/ CNC-GO/ CNC-GO-PLA-MWCNT was a physico-chemical process, according to the results.

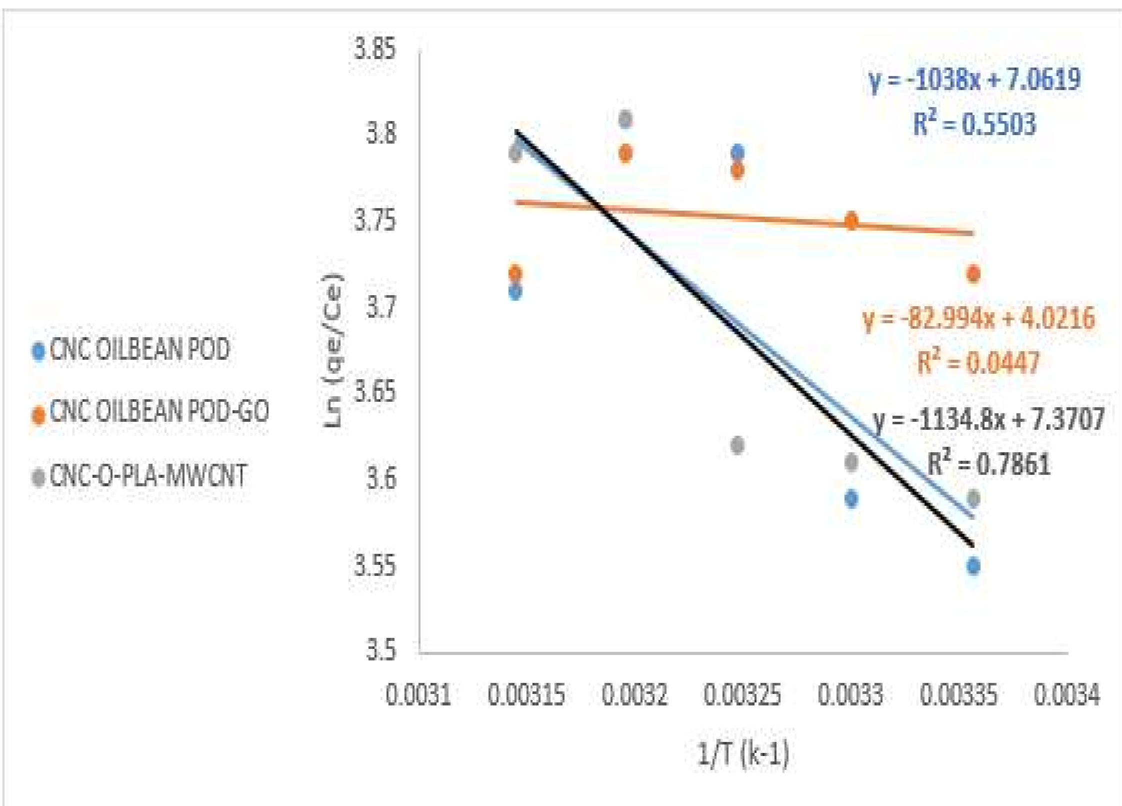

Figure 16: Thermodynamic plot for Pb ion adsorption onto CNC oilbean pod, CNC-GO and CNC-GO-PLA-MWCNT

Table 1 Results of isotherm plot parameters for adsorption of lead ion

METAL ION	ADSORBENT	LANGMUIR q_m(mg/g)	K_L(L/mg)	R^2	FREUNDLICH 1/*n*	K_F	R^2
	OILBEAN POD						
Pb	CNC	111.1	0.0046	0.8859	1.064	1.2852	0.9998
	CNC-GO	136.9	0.0037	0.8113	1.053	1.2912	0.9999
	CNC-GO-PLA-MWCNT	40	0.0173	0.7101	1.239	1.0552	0.995

METAL ION	ADSORBENT	TEMKIN B (j/mol)	Kt (L/g)	R^2	DUBININN- RADUSHKEVICH q_D (mg/g)	R^2	β (mol^2 /kJ^2)
	OILBEAN POD						
	CNC	5.663	6.6088	0.9287	10.030	0.8168	5E-06
	CNC-GO	5.7165	6.6606	0.9242	10.091	0.8191	5E-06
	CNC-GO-PLA-MWCNT	4.8305	3.806	0.8904	9.368	0.7565	2E-06

Table 2. Results of kinetics plot parameters for adsorption of lead ion

PARAMETERS	OILBEAN POD CNC	CNC-GO	CNC-GO PLA - MWCNT
Pseudo first order			
K_1 (min) $^{-1}$	0.0577	0.0409	0.0159
q_e (mg/g)	1.2125	3.6752	2.8354
R^2	0.917	0.7891	0.6282
Pseudo second order			
K_2 (g/mg min)	0.56	0.2734	0.2528
q_e (mg/g) experimental	4.0917	4.0290	4.0388
R^2	0.9999	0.9999	1
Elovich model			
α (mg/min)	3.2563	3.5309	3.6236
β (g/mg)	0.1649	0.1025	0.0838
R^2	0.9476	0.818	0.9447
Intra particle diffusion model			
K_{id}	0.045	0.027	0.0225
C (mg g-1)	3.5772	3.738	3.7896
R^2	0.9379	0.7521	0.9041

Table 3. Results of thermodynamic plot parameters for adsorption of lead ion

ADSORBENT	T/K	ΔG°/kJ mol^{-1}	ΔH°/kJ mol^{-1}	ΔS°/J K^{-1} mol^{-1}	R^2
OILBEAN POD					
CNC	298	-8.795			
	303	-9.044			
	308	-9.705	124.85	-0.849	0.5503
	313	-9.889			
	318	-9.809			
CNC -GO	298	-9.217			
	303	-9.447			
	308	-9.679	9.982	-0.484	0.0447
	313	-9.863			
	318	-9.835			
CNC –GO-PLA-MWCNT	298	-8.787			
	303	-9.094			
	308	-9.269			
	313	-9.915	136.49	-0.887	0.7861
	318	-10.02			

Conclusion

The utilization of environmentally friendly synthesis methods to create affordable biopolymers as substitute adsorbents for metal ion biosorption in aqueous solutions has garnered more attention in recent years. Because cellulose nanomaterials offer enormous chemical and mechanical potentials above their bulk equivalents, they have demonstrated exceptional performance in nearly all sectors of research and engineering. Through batch adsorption tests, the removal of Pb from aqueous solution has been investigated utilizing CNC, CNC-GO, and CNC-GO-PLA-MWCNT. Modifications in the pH of the solution, the dose of the adsorbent, and the duration of contact between the adsorbents and the adsorbates all had an impact on the adsorption capacity. The adsorption kinetics research showed that the pseudo-second order model best explained the data for metal ions. On the other hand, isotherm studies showed that the Freundlich model best explained the equilibrium data obtained for all processes, indicating heterogeneous adsorbate coverage onto the adsorbents' active sites. All adsorption process proved to be efficient. CNC-GO-PLA-MWCNT's nanocomposites recorded the best adsorption ability for the removal of lead ion, having an increased surface area and available complexation sites compared to CNC and CNC-GO. The negative ΔG° and ΔS° implied the spontaneous nature and effectiveness of the reaction. This suggests that the modification of CNC polymer nanocomposites gave an adsorbent that is highly effective as well as feasible for the removal of Pb (II) ion contamination from polluted wastewaters.

Authors contributions EPM: Designed the study; Wrote the first draft of the manuscript; Morphological analysis. ONM: Wrote the literature studies; Performed the synthesis, and Adsorption studies.

Funding There was no funding.

Data availability No datasets were generated or analyzed during the current study.

Declarations

Ethics approval and consent to participate Not applicable

Consent for publication Not applicable

Competing interests The authors declare no competing interest

REFERENCES

1. Guo, C.; Li, J.; Sun, Y.; Gao, W.; Mao, Z.; Ye, S. Influence of Constructed Rapid Infiltration System on Groundwater Recharge and Quality. *Front. Environ. Sci*. **2022**, 10:1022970. https://doi.org/10.3389/fenvs.2022.1022970

2. Meenakshi, A.; Timothy, D. F.; Matthew, J. B.; Andrew, W. W.; Chui, F.Y.; Peter, J. P.; Robert, B. J. The Infuence of Storm Water Infltration on Downslope Groundwater Chemistry. *Environ. Geochem. Health* **2023,** 45:8489–8501 https://doi.org/10.1007/s10653-023-01732-3

3. Saikat, M.; , Arka, J. C.; Abu, M. T.; Talha, B. E.; Firzan, N.; Ameer, K.; Abubakr, M. I.; Mayeen, U. K.; Hamid, O.; Fahad, A. A.; Jesus S. Impact of Heavy Metals on the Environment and Human Health: Novel Therapeutic Insights to Counter the Toxicity. *J. King Saud Uni. – Sci.* **2022,** https://doi.org/10.1016/j.jksus.2022.101865

4. Sumanta, D.; Kaniz, W. S.; Ashwell, R. N.; Moupriya, M.; Indrani, C. Heavy Metal Pollution in the Environment and Its Impact on Health: Exploring Green Technology for Remediation. *Environ. Health Insights.* **2023,** 17: 1–10, https://doi.org/10.1177/11786302231201259

5. Luo, D.; Liang, Y.; Wu, H.; Li, S.; He, Y.; Du, J.; Chen, X.; Pu, S. Human-Health and Environmental Risks of Heavy Metal Contamination in Soil and Groundwater at a Riverside Site, China. *Processes* **2022**, 10, 1994. https://doi.org/10.3390/ pr10101994

6. Veer, S.; Ghufran, A.; Sonali, V.; Pinki, K.; Sanjay, K. C.; Sachchida, N. R.; Emanuel,V.; Ashish, K. Toxic Heavy Metal Ions Contamination in Water and Their Sustainable Reduction By Eco-Friendly Methods: Isotherms, Thermodynamics and Kinetics Study. *Sci. Rep*. **2024,** 14:7595, https://doi.org/10.1038/s41598-024-58061-3

7. Kafilat, A. B. Assessment of Heavy Metal Pollution in Nigerian Surface Freshwaters and Sediment: A Meta-Analysis Using Ecological and Human Health Risk Indices. *J. Contam. Hydrol*. **2023,** 256:104199, https://doi.org/10.1016/j.jconhyd.2023.104199

8. Wu, D.; Hu, Y.; Cheng, H.; Ye, X. Detection Techniques for Lead Ions in Water: A Review. *Molecules* **2023**, 28, 3601. https://doi.org/ 10.3390/molecules28083601

9. Kshyanaprava, R.; Alok, P. Lead Pollution: Impact on Environment and Human Health and Approach for a Sustainable Solution. *Environ. Chem. Ecotoxicol*. **2023,** 79–85 https://doi.org/10.1016/j.enceco.2023.02.001

10. Ain, A. B.; Fatin, M. I.; Shakirah, A. W.; Nur, A. Y. Physical and Biochemical Toxicity Assessment of Acute Lead Nitrate ($Pb(NO_3)_2$) Exposure on Liver Tissues of Clarias gariepinus. *J. Environ. Microbiol. Toxicol*. **2024**,12(1):14-22, https://doi.org/10.54987/jemat.v12i1.1000

11. Gusain, R., Kumar, N., Fosso-kankeu, E., & Ray, S. S. (2019). Efficient removal of Pb (II) and Cd (II) from industrial mine water by a hierarchical MoS2/SH-MWCNT nanocomposite. *ACS Omega.* **2019**, 4: 13922−13935, https://doi.org/10.1021/acsomega.9b01603

12. Jaishankar, M.; Tseten, T.; Anbalagan, N.; Mathew, B. B.; Beeregowda, K. N. Toxicity, Mechanism and Health Effects of Some Heavy Metals. *Interdiscip. Toxicol*. **2014**, 7(2):60-72, https://doi.org/10.2478/intox-2014-0009

13. Jonathan, A.; Benyade, K. B.; Fobi, E. O.; David, A.; Francis, O.; Lyndon, N. S.; Osei, A. A review of health hazards associated with exposure to galamsey-related pollutants. Health Sci. Investig. J. 2024 Volume 5 (Issue 2):726-734. https://doi.org/10.46829/hsijournal.2024.6.5.2.726-734

14. Samuel, M. C.; Senthil, K. V.; Naveensubramaniam, V.; Kanimozhi, V.; Muhammad, A. S.; Sibiya Staceya, R.G.; Jogannagari, A.; Rajan, C.; Vladislav, L.; Gabriel, I. T.; Fedor, S.; Sivasankar, K.; Sasikumar, S. Bioaccumulation of Lead (Pb) and Its Effects on Human: A Review. *J. Haz. Mat. Adv.* **2022,** https://doi.org/10.1016/j.hazadv.2022.100094

15. Chen, Z.; Aziz, T.; Sun, H. Advances and Applications of Cellulose Bio-Composites in Biodegradable Materials. *J Polym. Environ.* **2023,** 31: 2273–2284, https://doi.org/10.1007/s10924-022-02561-8

16. Marcio, S. A.; Otávio, H. I.; Robson, S. C.; Marcus, V.S.; Rita, C. R.; Esperidiana A. M. Development of Sustainable Food Packaging Material Based on Biodegradable Polymer Reinforced With Cellulose Nanocrystals. *Food Packag. Shelf Life.* **2022,** 31:100807, https://doi.org/10.1016/j.fpsl.2021.100807

17. Alipour, A.; Zarinabadi, S.; Azimi, I.; Mirzaei, M. Effective Removal of Heavy Metal Using Cellulose Nanocomposite Adsorbents: Response Surface Methodology. Iranian (Iranica) J. Energy Environ.2022, 13(3): 258-272, doi: 10.5829/ijee.2022.13.03.06

18. Bondeson, D.; Mathew, A.; Oksman, K. Optimization of the Isolation of Nanocrystals from Microcrystalline Cellulose by Acid Hydrolysis. *Cellulose*. **2006**, 13, 171-180, https://doi.org/10.1007/s10570-006-9061-4

19. Diem, L. N.; Torgbo, S.; Banerjee, I.; Pal, K.; Sukatta, U.; Rugthaworn, P.; Sukyai, P. Sugarcane Bagasse-Derived Cellulose Nanocrystal/Polyvinyl Alcohol/Gum Tragacanth Composite Film Incorporated with Betel Leaf Extract as a Versatile Biomaterial for Wound Dressing. *Int. J. Biomater.* **2023**, 9630168,

https://doi.org/10.1155/2023/9630168

20. Rashid, S.; Shahi, A.K.; Dutta, H. Extraction and Characterization of Cellulose and Cellulose Nanowhiskers from Almond Shell Biomass, Metal Removal and Toxicity Analysis. *Biointerface Res. Appl. Chem*. **2022**, 12:2, 1705 - 1720 http://doi.org/10.33263/BRIAC122.17051720

21. Oprica, G.M.; Panaitescu, D.M.; Lixandru, B.E.; Usurelu, C.D.; Gabor, A.R.; Nicolae, C.-A.; Fierascu, R.C.; Frone, A.N. Plant-Derived Nanocellulose with Antibacterial Activity for Wound Healing Dressing. *Pharmaceutics.* **2023**, 15, 2672, https://doi.org/10.3390/ pharmaceutics15122672

22. Feizi, Z.; Shakeri, A.; Fordoei, A. R. Investigation of Nanostructure's Morphology Extracted from Walnut Shell Using Hydrolysis Acid and Ball Milling Methods. *Preprints.org*. **2022**, https://doi.org/10.20944/preprints202203.0184.v3

23. Ogundare, S. A.; Moodley, V.; Amaku, J. F.; Ogunmoye, A. O. Nanocrystalline Cellulose Derived from Melon Seed Shell (Citrullus Colocynthis L) for Reduction and Stabilization of Silver Nanoparticles : Synthesis and Catalytic Activity Nanocrystalline Cellulose Derived from Melon Seed Shell (Citrullus Colocynthis). *Carbohyd. Polym. Technol. Appl.* **2023**,.*2*(5):100134. https://doi.org/10.1016/j.carpta.2021.100134

24. Ayach, J.; El Malti, W.; Duma, L.; Lalevée, J.; Al Ajami, M.; Hamad, H.; Hijazi, A. Comparing Conventional and Advanced Approaches for Heavy Metal Removal in Wastewater Treatment: An In-Depth Review Emphasizing Filter-Based Strategies. *Polym*. **2024**, 16, 1959. https://doi.org/10.3390/ polym16141959

25. Ajiboye, T.O.; Oyewo, O.A.; Onwudiwe, D.C. Conventional and Current Methods of Toxic Metals Removal from Water Using g-C_3N_4-Based Materials. *J. Inorg. Organomet. Polym*. **2021**, 31, 1419–1442, https://doi.org/10.1007/s10904-020-01803-3

26. Isa, M.H.; Wong, L.P.; Mubarak, N.M. Editorial: Advances in Removal of Toxic Substances from Wastewater. *Front. Environ. Sci.* **2023**, 11:1165882. doi: 10.3389/fenvs.2023.1165882

27. Wang, Q.; Zhu, S.; Xi, C.; Zhang, F. A Review: Adsorption and Removal of Heavy Metals Based on Polyamide-amines Composites. *Front. Chem.* **2022**, 1–15. https://doi.org/10.3389/fchem.2022.814643

28. Raji, Z.; Karim, A.; Karam, A.; Khalloufi, S. Adsorption of Heavy Metals: Mechanisms, Kinetics, and Applications of Various Adsorbents in Wastewater Remediation—A Review. *Waste* **2023**, 1, 775–805. https://doi.org/10.3390/ waste1030046

29. Liu, Z.; Li, X.; Xie, W.; Deng, H. Extraction, Isolation and Characterization of Nanocrystalline Cellulose from Industrial Kelp (*Laminaria japonica*) waste. *Carbohydr. Polym.* **2017**, 173, 353-359, https://doi.org/10.1016/j.carbpol.2017.05.079.

30. Tibolla, H.; Pelissari, F. M.; Martins, J. T.; Vicente, A. A.; Menegalli, F. C. Cellulose nanofibers produced from banana peel by chemical and mechanical treatments: Characterization and cytotoxicity assessment. Food Hydrocolloids, **2018**, 75, 192–201, https://doi.org/10.1016/j.foodhyd.2017.08.027

31. Schiavi, D.; Ronchetti, R.; Di Lorenzo, V.; Vivani, R.; Giovagnoli, S.; Camaioni, E.; Balestra, G.M. Sustainable Protocols for Cellulose Nanocrystals Synthesis from Tomato Waste and Their Antimicrobial Properties against *Pseudomonas syringae pv*. Tomato. Plants **2023**, 12, 939. https://doi.org/10.3390/ plants12040939

32. Junhong, T.; Jie, Y.; Chengxiao, M.; Junfeng, L.; Keqing, D.; Zhen, W.; Cuizhong, C.; Zhaoyang, W.; Chun, Z.; Xiaoya, D. Cellulose Nanocrystals/Graphene Oxide Composite for the Adsorption and Removal of Levofloxacin Hydrochloride Antibiotic from Aqueous Solution. *R. Soc. Open Sci*. **2020,** 7: 200857. http://dx.doi.org/10.1098/rsos.200857

33. Li, Y.; Dong, X.; Yao, L.; Wang, Y.; Wang, L.; Jiang, Z.; Qiu, D. Preparation and Characterization of Nanocomposite Hydrogels Based on Self-Assembling Collagen and Cellulose Nanocrystals. *Polymers* **2023**, 15, 1308. https://doi.org/ 10.3390/polym15051308

34. Al-Saeedi, S.I.; Areej, A.; Qamar, M.T.; Alhujaily, A.; Iqbal, S.; Alotaibi, M.T.; Aslam, M; Qayyum, M.A.; Bahadur, A., Awwad, N.S.; Jazaa, Y.; Elkaeed, E.B. Isotherm and Kinetic Studies for the Adsorption of Methylene Blue Onto a Novel Mn_3O_4- Bi_2O_3 Composite and Their Antifungal Performance. *Front. Environ. Sci.* **2023,** 11:1156475. doi: 10.3389/fenvs.2023.1156475

35. Ahmed, M.; Maysa, R. M.; Saied, A. M.; Gehad, G. M.; Omar, A. F. Kinetics and Adsorption Isotherms Studies for the Effective Removal of Evans Blue Dye from an Aqueous Solution Utilizing Forsterite Nanoparticles. *Scientific Reports*. **2024**, 14:24392, https://doi.org/10.1038/s41598-024-73697-x

36. Alamzeb, M.; Tullah, M.; Ali, S.; Ihsanullah; Khan, B.; Setzer, W.N.; Al-Zaqri, N.; Ibrahim, M.N.M. Kinetic, Thermodynamic and Adsorption Isotherm Studies of Detoxification of Eriochrome Black T Dye from Wastewater by Native and Washed Garlic Peel. *Water.* **2022**, 14, 3713. https://doi.org/10.3390/ w14223713

37. Ogundiran, A. A.; Ogundiran, O. O.; Badeji, A. A.; Osinubi A. D. Kinetic, Isotherm and Thermodynamic Studies of the Adsorption of Cresol Red Dye Using Agricultural Wastes. *Nig. J. Sci. Environ.* **2024**, 22 (2) 28–https://doi.org/10.61448/njse222243

38. Tao, J.; Yang, J.; Ma, C.; Li, J.; Du, K.; Wei, Z.; Deng, X. Cellulose Nanocrystals / Graphene Oxide Composite for the Adsorption and Removal of Levofloxacin Hydrochloride Antibiotic from Aqueous Solution. *R. Soc. Open Sci.* **2020**, 7, 200857. http://dx.doi.org/10.1098/rsos.200857.

39. Nsude, O. P., Orie, K. J., Udeozo, P. I., Ogbobe, O., & Chime, C. C. Isolation, Physicochemical and BET Analysis of Cellulose from Pentaclethra macrophylla Benth (Oil Bean) Pod Biomass Wastes. *Int. Res. J. Pure. Appl.Chem.* **2022**, 9–22. https://doi.org/10.9734/irjpac/2022/v23i530474

40. Baloyi, R.B.; Sithole, B.B. Chunilall, V. Physicochemical Properties of Cellulose Nanocrystals Extracted from Postconsumer Polyester/Cotton-Blended Fabrics and Their Effects on PVA Composite Films. *Polym. (Basel)*. **2024**, 24; 16(11):1495, doi: 10.3390/polym16111495

41. Somanathan, T., Prasad, K., Ostrikov, K.K., Saravanan, A., and Krishna, V.M. Graphene Oxide Synthesis from Agro Waste. *Nanomaterials* **2015**, 5, 826-834, https://doi.org/10.3390/nano5020826

42. Lasheen, M. R.; El-Sherif, I. Y.; Sabry, D. Y.; El-Wakeel, S. T.; El-Shahat, M. F. Removal of Heavy Metals from Aqueous Solution by Multiwalled Carbon Nanotubes: Equilibrium, Isotherms, and Kinetics. *Desalin. Water Treat*. **2015**, 53(13), 3521–3530. https://doi.org/10.1080/19443994.2013.873880

43. Yu, F.; Yanqing, W.; Jie, M.; Chi, Z. Adsorption of Lead on Multi-Walled Carbon Nanotubes with Different Outer Diameters and Oxygen Contents: Kinetics, Isotherms and Thermodynamics. *J. Environ. Sci.* **2013**, 25, 193 -205. doi: 10.1016/s1001-0742(12)60023-0

44. Jedla, M. R.; Koneru, B.; Franco, A.; Rangappa, D.; Banerjee, P. Recent Developments in Nanomaterials Based Adsorbents for Water Purification Techniques. *Biointerf. Res.Appl. Chem.* **2022**, 12(5), 5821–5835. https://doi.org/10.33263/BRIAC125.58215835

45. Ali, S. Z.; Athar, M.; Salman, M.; Din, M. I. Simultaneous Removal of Pb (II), Cd (II) and Cu (II) from Aqueous Solutions by Adsorption on Triticum aestivum – A Green Approach. *Hydrol. Curr. Res*. **2011**, 2 (4), 118–125, https://doi.org/10.4172/2157-7587.1000118

46. Kang, S., Mauter, M.S., Elimelech, M. Microbial Cytotoxicity of Carbon-Based Nanomaterials: Implications for River Water and Wastewater Effluent. Environ. Sci. Technol. 2009, 43, 2648 2653, https://doi.org/10.1021/es8031506

47. Bharathi, K. S.; Rameshsrikrishna, P. (2012). Equilibrium, Thermodynamic and Kinetic Studies on Adsorption of a Basic Dye by Citrullus lanatus Rind. *Iranica J. Energy Environ*. 3(1), 23-34, http://dx.doi.org/10.5829/idosi.ijee.2012.03.01.0130

48. Manjuladevi, M.; Sri, O. M. Heavy Metals Removal from Industrial Wastewater by Nano Adsorbent Prepared from Cucumis Melopeel Activated Carbon. J Nanomed Res. **2017,** 5(1), 00102, DOI: 10.15406/jnmr.2017.05.00102

49. Ali, R. M.; Hamad, H. A.; Hussein, M. M.; Malash, G. F. Potential of Using Green Adsorbent of Heavy Metal Removal from Aqueous Solutions: Adsorption Kinetics, Isotherm, Thermodynamic, Mechanism and Economic Analysis. *Ecol. Eng.* **2016,** 91: 317–332, https://doi.org/10.1016/j.ecoleng.2016.03.015

50. Dada, A.; Olalekan, A.; Olatunya, A.; Dada, O. Langmuir, Freundlich, Temkin and Dubinin-Radushkevich Isotherms Studies of Equilibrium Sorption of Zn^{2+} unto Phosphoric Acid Modified Rice Husk. J. Appl. Chem. 2012, 3, 38–45, http://doi.org/10.9790/5736-0313845

51. Temkin, M.; Pyzhev, V. Heavy Metals Removal and Isotherms Study. *Acta Physiochimca URSS.* 1940, 12, 217–222.

52. Freundlich, H.M.F. Over the Adsorption in Solution. *Zeitschrift Physikalishche Chemie*. 1906, 57, 385-470.

53. Qiao, J.; Gao, S.; Yao, J.; Zhang, L.; Li, N. A Rapid and Green Method for the Removal of Anionic Dyes from Aqueous Solution Using Sulfobetaine-Modified Magnetic Nanoparticles. *AIP Adv.* **2019**, 9, 065308, https://doi.org/10.1063/1.5101013

54. Soliman, E. M.; Ahmed, S. A.; Fadl, A. A. Adsorptive Removal of Oil Spill from Sea Water Surface Using Magnetic Wood Sawdust as A Novel Nano-Composite Synthesized Via Microwave Approach. *J Environ Health Sci Eng.* **2020**,18, 79–90, https://doi.org/10.1007/s40201-019-00440-

55. Ouyang, D.; Zhuo, Y.; Hu, L.; Zeng, Q.; Hu, Y.; He, Z. Research on the Adsorption Behavior of Heavy Metal Ions by Porous Material Prepared with Silicate Tailings. *Minerals* **2019**, *9*, 291. https://doi.org/10.3390/min9050291

56. Xu, H.; Zhang, Y.; Tang, J.; Tian, W.; Zhao, Z.; Chen, Y. Removal of Cationic Dyes from Aqueous Solutions Using Adsorbents Based on GO / APTG Nanocomposites. *Desalin. Water Treat*. **2020**, 174, 414–427. https://doi.org/10.5004/dwt.2020.24888

57. Farooq, S.; Aziz, H.; Ali, S.; Murtaza, G.; Rizwan, M.; Saleem, M.H.; Mahboob, S.; Al-Ghanim, K.A.; Riaz, M.N.; Murtaza, B. Synthesis of Functionalized Carboxylated Graphene Oxide for the Remediation of Pb and Cr Contaminated Water. *Int. J. Environ. Res. Public Health* **2022**, *19*, 10610. https://doi.org/10.3390/ijerph191710610

58. Yakubu, A; Olatunji; G. A; Adekola, F. A. Modified/Unmodified Nanoparticle Adsorbents of Cellulose Origin With High Adsorptive Potential for Removal of Pb(II) From Aqueous Solution. *Eur Sci J ESJ*. **2017**, 13(27):425–425, https://doi.org/10.19044/esj.2017.v13n27p425